

Experimental simulation of quantum graphs by microwave networksOleh Hul,¹ Szymon Bauch,¹ Prot Pakoński,² Nazar Savytskyy,¹ Karol Życzkowski,^{2,3} and Leszek Sirko¹¹*Institute of Physics, Polish Academy of Sciences, Aleja Lotników 32/46, 02-668 Warszawa, Poland*²*Instytut Fizyki im. Smoluchowskiego, Uniwersytet Jagielloński, ul. Reymonta 4, 30-059 Kraków, Poland*³*Center for Theoretical Physics, Polish Academy of Sciences, Aleja Lotników 32/46, 02-668 Warszawa, Poland*

(Received 28 August 2003; published 11 May 2004)

We present the results of experimental and theoretical study of irregular, tetrahedral microwave networks consisting of coaxial cables (annular waveguides) connected by T joints. The spectra of the networks were measured in the frequency range 0.0001–16 GHz in order to obtain their statistical properties such as the integrated nearest neighbor spacing distribution and the spectral rigidity $\Delta_3(L)$. The comparison of our experimental and theoretical results shows that microwave networks can simulate quantum graphs with time reversal symmetry. In particular, we use the spectra of the microwave networks to study the periodic orbits of the simulated quantum graphs. We also present experimental study of directional microwave networks consisting of coaxial cables and Faraday isolators for which the time reversal symmetry is broken. In this case our experimental results indicate that spectral statistics of directional microwave networks deviate from predictions of Gaussian orthogonal ensembles in random matrix theory approaching, especially for small eigenfrequency spacing s , results for Gaussian unitary ensembles. Experimental results are supported by the theoretical analysis of directional graphs.

DOI: 10.1103/PhysRevE.69.056205

PACS number(s): 05.45.Mt, 03.65.Nk

Quantum graphs of connected one-dimensional wires were introduced more than 50 years ago in order to describe organic molecules by free electron models [1,2]. They can be considered as idealizations of physical networks in the limit where the widths of the wires are much smaller than their lengths, i.e., assuming that the propagating waves remain in a single transversal mode. Among the systems modeled by quantum graphs one can find, e.g., electromagnetic optical waveguides [3,4], quantum wires [5,6], mesoscopic systems [7,8], and excitation of fractons in fractal structures [9,10]. In spite of the attention paid to quantum graphs, the statistical properties of their spectra were hardly investigated in the past. Recently spectral properties of quantum graphs have been studied in the series of papers by Kottos and Smilansky [11–13]. They have shown that quantum graphs are excellent paradigms of quantum chaos. However, in spite of numerous theoretical investigations of this topic [14–21] no experiments have been performed so far.

The main aim of this work is to demonstrate that using a simple experimental setup consisting of microwave networks (throughout the text we also use the names: microwave graphs or circuits) one may successfully simulate quantum graphs. The circuits are constructed of coaxial cables (annular waveguides) connected by T joints. Furthermore, to mimic the effects of the time reversal symmetry breaking in quantum systems it is sufficient to add the Faraday isolators into the circuit.

The analogy between quantum graphs and microwave networks is based upon the equivalency of the Schrödinger equation describing the quantum system and the telegraph equation describing the ideal microwave circuit. It is worth noting that this paper continues the use of microwave spectroscopy to verify wave effects predicted on the basis of quantum physics, which for two-dimensional systems, thin microwave cavity resonators, was pioneered in Ref. [22] and further developed in Refs. [23–28]. The first microwave ex-

periment specifically devoted to the study of quantum chaotic scattering was reported in Ref. [29]. Later on a similar experimental technique was applied in the observation of resonance trapping in an open microwave cavity [30]. In the case of two dimensions the Schrödinger equation for quantum billiards is equivalent to the Helmholtz equation for microwave cavities of corresponding shape. Three-dimensional chaotic billiards have been also studied experimentally in the microwave frequency domain [31,32] but for these systems there is no direct analogy between the vectorial Helmholtz equation and the Schrödinger equation.

A general microwave graph consists of N vertices (T joints in our case) connected by bonds, e.g., coaxial cables. Following Ref. [12] we define the $N \times N$ connectivity matrix C_{ij} which takes the value 1 if the vertices i and j are connected and 0 otherwise. The coaxial cable consists of an inner conductor of radius r_1 surrounded by a concentric conductor of inner radius r_2 . The space between the inner and the outer conductors is filled with a homogeneous material having the dielectric constant ϵ . For frequency ν below the onset of the next TE_{11} mode [33], inside a coaxial cable only the fundamental TEM mode can propagate, which in the literature it often called a Lecher wave. This mode exists because the cross section of a coaxial line is doubly connected, which results in the existence of the potential difference between the inner and the outer conductors [see Eq. (2)].

In order to find propagation of a Lecher wave inside the coaxial cable joining the i th and the j th vertex of the microwave graph we can begin with the continuity equation for the charge and the current on the considered cable (bond) [34]

$$\frac{de_{ij}(x,t)}{dt} = -\frac{dJ_{ij}(x,t)}{dx}, \quad (1)$$

where $e_{ij}(x,t)$ and $J_{ij}(x,t)$ are the charge and the current per unit length on the surface of the inner conductor of a coaxial cable.

For the potential difference we can write down

$$U_{ij}(x,t) = V_2^{ij}(x,t) - V_1^{ij}(x,t) = \frac{e_{ij}(x,t)}{C}, \quad (2)$$

where $V_1^{ij}(x,t)$ and $V_2^{ij}(x,t)$ are the potentials of the inner and the outer conductors of a coaxial cable and C is the capacitance per unit length of a cable.

Taking the spatial derivative of Eq. (2) and assuming that the wave propagating along the cable is monochromatic $e_{ij}(x,t) = e^{-i\omega t} e_{ij}(x)$ and $U_{ij}(x,t) = e^{-i\omega t} U_{ij}(x)$ one can obtain [34]

$$\frac{d}{dx} U_{ij}(x) = -Z J_{ij}(x), \quad (3)$$

where $Z = \mathcal{R} - (i\omega \mathcal{L}/c^2)$. \mathcal{R} and \mathcal{L} denote the resistance and the inductance per unit length, respectively. The angular frequency ω is equal to $2\pi\nu$ and c stands here for the speed of light in a vacuum.

Making use of Eqs. (1)–(3) and the definition of Z for an ideal lossless coaxial cable with the resistance $\mathcal{R}=0$, one can derive the telegraph equation on the microwave graph

$$\frac{d^2}{dx^2} U_{ij}(x) + \frac{\omega^2 \varepsilon}{c^2} U_{ij}(x) = 0, \quad (4)$$

where $\varepsilon = \mathcal{L}C$ [35].

The continuity equation for the potential difference requires that for every $i=1, \dots, N$

$$U_{ij}(x)|_{z=0} = \varphi_i, \quad U_{ij}(x)|_{z=L_{ij}} = \varphi_j, \quad i < j, \quad C_{ij} \neq 0. \quad (5)$$

The current conservation condition

$$\sum_{j < i} C_{ij} J_{ji}(x)|_{x=L_{ij}} - \sum_{j > i} C_{ij} J_{ij}(x)|_{x=0} = 0 \quad (6)$$

may be transformed using Eq. (3) into

$$-\sum_{j < i} C_{ij} \frac{d}{dx} U_{ji}(x)|_{x=L_{ij}} + \sum_{j > i} C_{ij} \frac{d}{dx} U_{ij}(x)|_{x=0} = 0, \quad (7)$$

where L_{ij} represents the length of the bond joining the i th and the j th vertex of the graph. To simplify the notation, the lengths of six bonds of the four-vertex graph shown in Fig. 1 are labeled by letters $\{a, \dots, f\}$.

Assuming the following correspondence: $\Psi_{ij}(x) \Leftrightarrow U_{ij}(x)$ and $k^2 \Leftrightarrow \omega^2 \varepsilon / c^2$, Eq. (4) is formally equivalent to the one-dimensional Schrödinger equation (with $\hbar = 2m = 1$) on the graph with the magnetic vector potential $A_{ij} = 0$ [12],

$$\frac{d^2}{dx^2} \Psi_{ij}(x) + k^2 \Psi_{ij}(x) = 0. \quad (8)$$

It is easy to verify that Eqs. (5) and (7) are equivalent to equations derived in Ref. [12] [see Eq. (3)] for quantum graphs with Neumann boundary conditions ($\lambda_i = 0$) and vanishing magnetic vector potential $A_{ij} = A_{ji} = 0$. Such systems possess the time reversal symmetry (TRS),

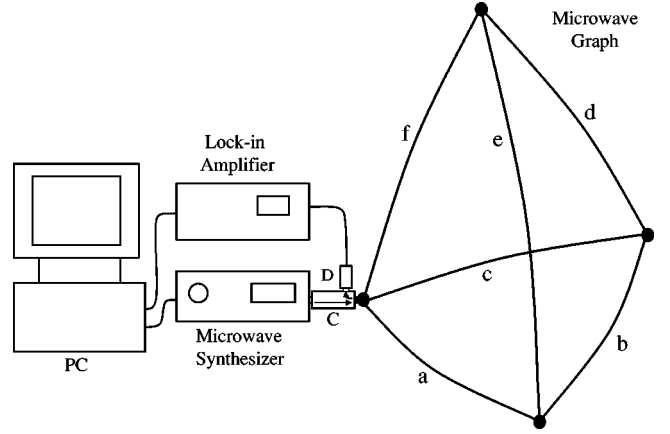


FIG. 1. Experimental setup for measurements of the spectra of the microwave graphs. Microwave synthesizer: HP8672A (2–18.5 GHz) and SMT03 (5 kHz–3 GHz), D - crystal detector (HP8472B), C - microwave coupler (Narda 4055).

$$\begin{aligned} \Psi_{ij}(x)|_{x=0} = \varphi_i, \quad \Psi_{ij}(x)|_{x=L_{ij}} = \varphi_j, \quad i < j, \quad C_{ij} \neq 0 \\ -\sum_{j < i} C_{ij} \frac{d}{dx} \Psi_{ji}(x)|_{x=L_{ij}} + \sum_{j > i} C_{ij} \frac{d}{dx} \Psi_{ij}(x)|_{x=0} = 0. \end{aligned} \quad (9)$$

In order to check the equivalence of microwave and quantum graphs we measured the spectra of ten tetrahedral microwave graphs in the frequency range 0.0001–16 GHz. For this frequency range only a Lecher wave can propagate in the graphs. The next mode to propagate is the TE_{11} with the cutoff frequency $\nu_c \approx c / \pi(r_1 + r_2) \sqrt{\varepsilon} = 32.9$ GHz [33], where $r_1 = 0.05$ cm is the inner wire radius of the coaxial cable (SMA-RG402), while $r_2 = 0.15$ cm is the inner radius of the surrounding conductor, and $\varepsilon = 2.08$ is Teflon dielectric constant.

The experimental setup for measurements of spectra of the microwave graphs is shown in Fig. 1. We used Hewlett-Packard 8672A microwave synthesizer to measure the spectra of the graphs in the frequency range 2–16 GHz while for the frequency range 0.0001–3 GHz Rhode-Schwartz SMT-03 microwave synthesizer was used. The microwave coupler (Narda 4055) enabled us to observe signals reflected from microwave graphs. Because for the specified frequency range only a single TEM mode could propagate in the microwave networks a reflected signal was proportional to $|S|^2$, where the complex number S may be considered as a one-dimensional scattering matrix. This type of microwave experiment, related to scattering matrix measurements, was pioneered in Ref. [29] and stimulated in Ref. [36]. In Fig. 2(a) a typical fragment of a measured modulus of scattering matrix $|S|$ of the graph is presented in the frequency range 3.95–5.05 GHz. The experimental spectrum is also compared with numerically calculated eigenfrequencies of the ideal graph ($R=0$) having the same bond lengths as the experimental one. The total “optical” lengths of the microwave graphs, including T joints, varied from 171.7 to 262.2 cm, which allowed for the observation of 156–264 eigenfrequencies in the frequency range 0.0001–16 GHz. To avoid the degeneracy of eigenvalues the lengths $L_{i,j}$ of the bonds

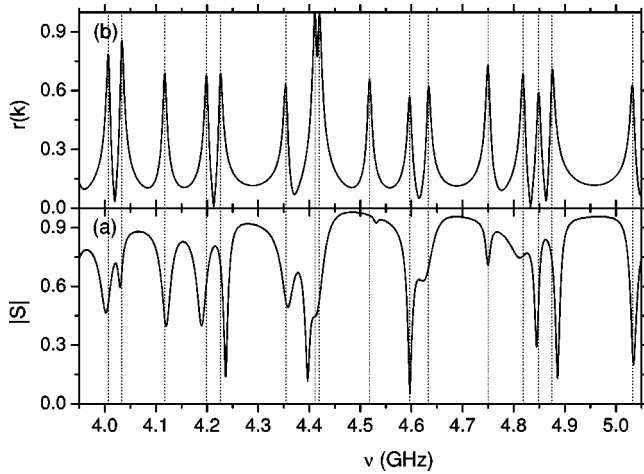


FIG. 2. (a) A fragment of a measured modulus of scattering matrix $|S|$ of the microwave graph of the “optical” length 223.6 cm in the frequency range 3.95–5.05 GHz (b) The response function $r(k)$ calculated for the graph having the same bond lengths as the experimental one. In the calculations of the response function $r(k)$ absorption of the microwave field by coaxial cables were taken into account (see text). Vertical broken lines show the positions of numerically calculated eigenfrequencies of the graph without absorption.

(cables) were chosen not to be commensurable. The transmission through the T joints was characterized by the weak frequency dependence, e.g., in the frequency range 0.05–16 GHz the ratio $R_S = (|S_{ij}|^{\max} - |S_{ij}|^{\min}) / |S_{ij}|^{\max} \leq 0.06$, where $|S_{ij}|^{\max}$ and $|S_{ij}|^{\min}$ are the maximum and the minimum values of modulus of nondiagonal elements of a three port scattering matrix S_{ij} , respectively. The indices $i, j = 1, 2, 3$ and $i \neq j$. For the frequency range 3.95–5.05 GHz specified in Fig. 2(a) the ratio fulfilled the condition $R_S \leq 0.02$.

For more comprehensive comparison of the experimental and numerical results the experimental spectrum shown in Fig. 2(a) is compared in Fig. 2(b) with the response function $r(k)$ calculated for the graph having the same bond lengths as the experimental one. The response function $r(k)$ was introduced in this paper in order to analyze the directional graphs consisting of Faraday isolators and is defined by Eq. (19). In the calculations of the response function $r(k)$ absorption of microwave cables were taken into account by replacing the real wave vector k by the complex vector $k + i\beta\sqrt{k}$ [35]. The absorption coefficient $\beta = 0.009m^{-1/2}$ was evaluated on the basis of absorption of the microwave cables used in the experiment. The direct comparison of the results presented in Figs. 2(a) and 2(b) requires some care because the response function $r(k)$ is rather proportional to the amplitude of the field transmitted through the graph than to the amplitude reflected from the graph that is represented by the scattering matrix $|S|$. However, the aim of this comparison is to show that the inclusion of absorption of microwave cables leads to comparable with the experimental results broadening of resonances. It is also important to note that calculated in such a way eigenfrequencies are very close to the ones calculated for the ideal graph, from which they differ at most by 1 MHz. Figures 2(a) and 2(b) show that the agreement be-

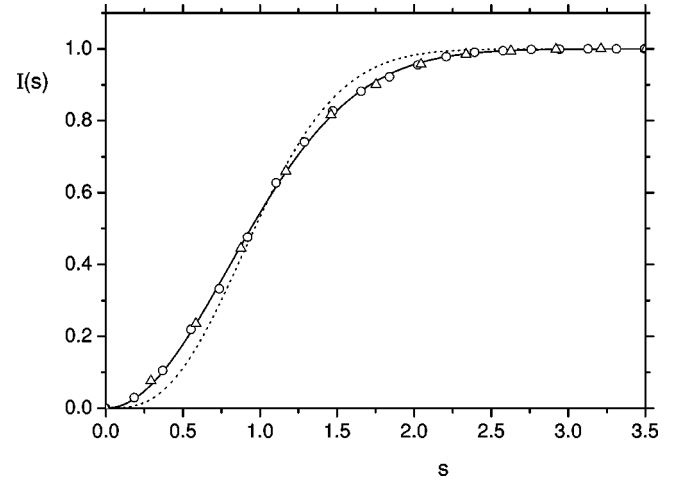


FIG. 3. Integrated nearest neighbor spacing (INNS) distribution $I(s)$ averaged for ten microwave graphs. Results of the experiment (open triangles) are compared with the numerical results (open circles) and theoretical prediction for GOE (solid line) and GUE (dashed line).

tween experimental and theoretical results is quite good (the relative errors are of the order of 10^{-3}), which justifies a posteriori our assumption that the microwave circuits can be described with good accuracy by the quantum graphs with Neumann boundary conditions. In this way our experimental results additionally support theoretical findings about the boundary conditions for shrinking domains [37,38]. Our results also show that relatively short microwave graphs consisting of coaxial cables, at least as it concerns the eigenvalues’ positions, can be approximately treated as ideal lossless graphs with the resistance $\mathcal{R} = 0$. The last statement is not very surprising. A similar situation one can find in the experiments with microwave cavities [22]. A thorough discussion on influence of absorption of energy caused by the finite conductivity of the cavity walls on reflection from the cavity power was given by Doron *et al.* [29]. They showed (see also Ref. [30]) that small absorption of energy is necessary for revealing cavity’s resonances as dips in the reflected power.

We have examined statistical properties of spectra of the microwave graphs such as the integrated nearest neighbor spacing (INNS) distribution $I(s)$ and the spectral rigidity $\Delta_3(L)$. (for their definitions see, e.g., Refs. [39,40]). Figure 3 presents the INNS distributions. The solid line represents predictions of random matrix theory obtained for Gaussian orthogonal ensemble (GOE), applicable for systems with a time-reversal symmetry. The dashed line denotes results characteristic of Gaussian unitary ensemble (GUE), used if the time-reversal symmetry is broken [39]. Experimental curve (open triangles) was obtained by averaging over the set of ten microwave graphs obtained by varying the length of one bond, which provided us with a total of 2220 experimentally measured eigenfrequencies. Numerical curve (open circles) shows results averaged for ten quantum graphs having the same bond lengths as the experimental ones. Eigenfrequencies were calculated by solving numerically the secular equations for quantum graphs [Eqs. (6)-(8) in Ref. [12]]. This procedure allowed us to identify a total of 2344 eigen-

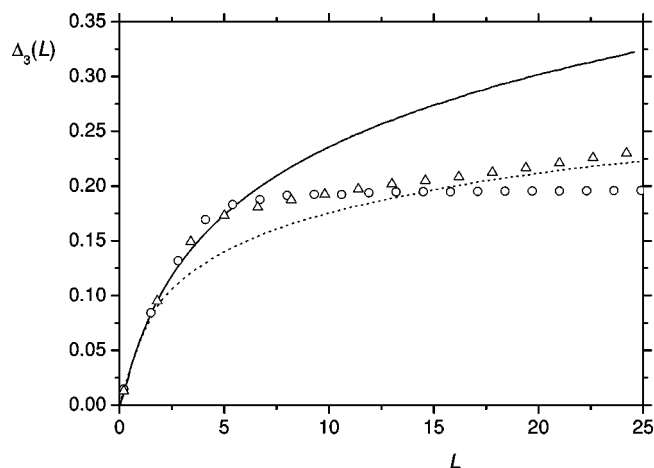


FIG. 4. Spectral rigidity $\Delta_3(L)$ for the microwave graph of the “optical” length 223.6 cm. Results of the experiment (open triangles) are compared with the numerical results (open circles) and theoretical prediction for GOE (solid line) and GUE (dashed line).

frequencies, slightly more than measured experimentally. Figure 3 shows that in both cases the INNS distributions are in a very good agreement with the GOE predictions.

Figure 4 demonstrates the spectral rigidity $\Delta_3(L)$ obtained for the microwave graph of the “optical” length 223.6 cm. Experimental curve (open triangles) was based on 229 identified eigenfrequencies, while the numerical data (open circles) were computed out of 237 eigenfrequencies. In both cases the frequency range was 0.0001–16 GHz. Deviations of the experimental and numerical rigidity from the GOE predictions (solid line) are visible. For comparison the dashed line in Fig. 4 shows the RMT prediction for GUE. Our experimental and numerical results are lying above the GOE prediction for L between 2.5–5. For higher value of L a saturation of the numerical value of the spectral rigidity is observed in agreement with the predictions of Berry [42]. The experimental rigidity for $L > 10$ is located below the GOE curve and above the numerical results. The departure of the experimental rigidity from the numerical one can be probably attributed to the loss of about 3 % of experimental eigenfrequencies.

The measurements of the spectra of the graphs enabled us also to calculate the lengths of periodic orbits in the graph. They were computed from the Fourier transform

$$F(l) = \int_0^{k_{max}} \tilde{\rho}(k) \omega(k) e^{-ikl} dk, \quad (10)$$

where $\tilde{\rho}$ is the oscillating part of the level density and $\omega(k) = \sin^2(\pi k/k_{max})$ is a window function that suppresses the Gibbs overshoot phenomenon [28,41]. Here k_{max} is the maximal value of the wave number within the interval where the eigenvalues of the graph were evaluated. In order to extract the oscillating part of the level density $\tilde{\rho}$ we determined the density of states according to $\rho(k) = \sum_j \delta(k - k_j)$ and subtracted from it the mean density $\bar{\rho}(k) = d\bar{N}(k)/dk$. The mean $\bar{N}(k)$ of the staircase function, i.e., the number of resonances up to the wave number k , was

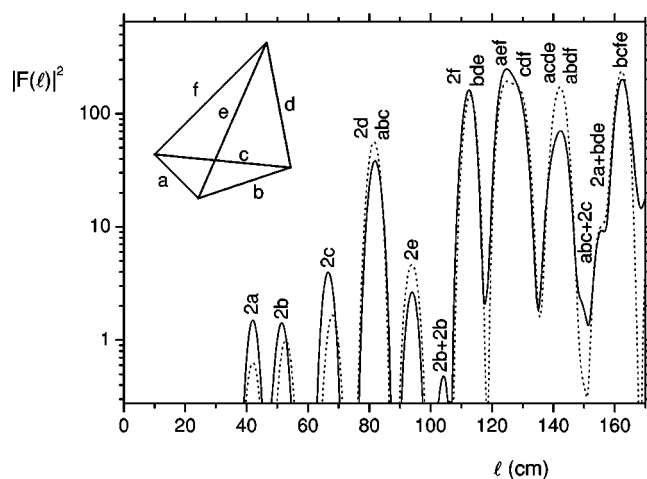


FIG. 5. Absolute square of the Fourier transform of the fluctuating part of the density of resonances of the graph of the “optical” length 223.6 cm. Results of the experiment (solid line) are compared with the numerical results (dotted line). The assignment of peaks of $|F(l)|^2$ to simple periodic orbits (see text) is shown along with the length of the orbits. The “optical” lengths of the bonds of the graph: $a=21.0$ cm, $b=26.3$ cm, $c=34.0$ cm, $d=39.6$ cm, $e=46.8$ cm, $f=55.9$ cm.

obtained from a least squares fit $\bar{N}(k) = \alpha_1 k + \alpha_2$ of the measured staircase $N(k)$. The slope parameter, obtained from the experimental data, $\alpha_1 = 0.707 \pm 0.006$, is very close to the value $\alpha = 0.712$, received from the Weyl formula given by Eq. (7) in Ref. [11].

The absolute square of the Fourier transform of the fluctuating part of the density of resonances $|F(l)|^2$ for the graph of the “optical” length 223.6 cm is shown in Fig. 5. The lengths of this graph fulfill the following relations: $a < b < c < d < e < f$. Results obtained from the experimental spectrum (solid line) are compared to the results obtained from numerical calculations (dotted line). The experimental spectrum included 149 identified eigenfrequencies while the numerical one included 150 eigenfrequencies. In both cases the frequency range was 0.2–10.2 GHz. We used the narrower frequency range than in the calculations of the INNS distributions and $\Delta_3(L)$ to be sure that at most only one eigenfrequency was missing in the experimental spectrum. The absolute square of the Fourier transform $|F(l)|^2$ shows pronounced peaks near the lengths of certain periodic orbits. The agreement between the experimental and the numerical results is good, however, some discrepancies for shorter periodic orbits are visible. In Fig. 5 we show all irreducible periodic orbits [12], i.e., periodic orbits which do not intersect themselves, with the lengths $l < 165$ cm. For clarity, in Fig. 5 we additionally show the first repetition of the periodic orbit $2b$ at $l = 2b + 2b = 105.2$ cm and two reducible periodic orbits $abc + 2c$ and $bde + 2a$ at $l = 149.3$ cm and $l = 154.7$ cm, respectively. It should be noticed that many peaks for $l > 70$ cm cover several unresolved periodic orbits. In order to check whether the missed resonance was responsible for discrepancies in the lengths of periodic orbits we artificially added this resonance to the spectrum of the graph and recalculated the lengths of periodic orbits (results are not

shown). Indeed, the inclusion of the missed level improved the agreement with the numerical results. The main change was visible in the “experimental” amplitudes that became closer to the numerical ones. For example the amplitudes of the most sensitive orbits $2a$ and $2b$ (see Fig. 5) were decreased from 1.5 to 1.0 and from 1.4 to 1.1, respectively. The positions of the periodic orbits were not as sensitive as amplitudes. For example in the case of the orbit $2a$ the length was changed from $\ell=42.0$ cm to $\ell=41.4$ cm becoming more distant from the numerical result $\ell=42.0$ cm. In a different way behaved the orbit $2b$ whose length was modified from $\ell=51.5$ cm to $\ell=52.5$ cm becoming closer to the numerical result $\ell=52.6$ cm.

In this paper we also present experimental study of microwave graphs consisting of coaxial cables and Faraday isolators. The graphs with Faraday isolators are examples of simple experimental realization of directional graphs for which the time reversal symmetry is broken. A microwave Faraday isolator is a passive device, which transmits the wave moving in one direction while absorbing the wave moving in the opposite direction. Due to absorption the introduction of Faraday isolators transforms the problem from the bound system to an open system. In the experiment AerCom 60583 Faraday isolators (insertion loss <0.4 dB, isolation >19 dB, length=5.7 cm) with the operating frequency range 3.5–7.5 GHz were used. We measured the spectra of four graphs consisting of one of their bonds’ one Faraday isolator or two Faraday isolators connected in series. The limitations imposed by the narrow range of isolators operating frequency lead to rather poor eigenfrequency statistics—between 34 and 39 eigenfrequencies were observed for the graphs with Faraday isolators. Therefore, for each of four graphs we performed three measurements where: the isolator was mounted in the bond b of the graph, the isolator was mounted in the bond d , and two isolators connected in series were mounted in the bond d . The assignment of the letters to the bonds of the graph is shown in Fig. 1.

The results of these 12 measurements (together 444 eigenfrequencies) were averaged to obtain the INNS distribution (solid triangles in Fig. 6). The INNS distribution obtained for the same frequency range, but without Faraday isolators are also shown in Fig. 6 (open triangles). The examination of the INNS distribution obtained for the graphs, with and without Faraday isolators, shows that they are different. In spite of some deviations, one can see that INNS distribution for the graphs without the isolators is close to the RMT prediction for GOE (solid line) in contrast to the INNS distribution for the graphs with the isolators, which follows more closely the RMT prediction for GUE (dashed line). This is especially well seen at small eigenfrequency spacing s . Similar deviations of the spectral statistics were reported by experiments with microwave billiards [25–27]. In the experiment performed by So *et al.* [25] the transition from GOE to GUE statistics was caused by a piece of magnetized ferrite placed inside a two-dimensional microwave cavity while in the experiment performed in Marburg [26,27] the deviation from GOE statistics was induced by Faraday isolator connected to a microwave cavity.

The directed graphs can be also modeled theoretically. The crucial element of the graph—the Faraday isolator in a

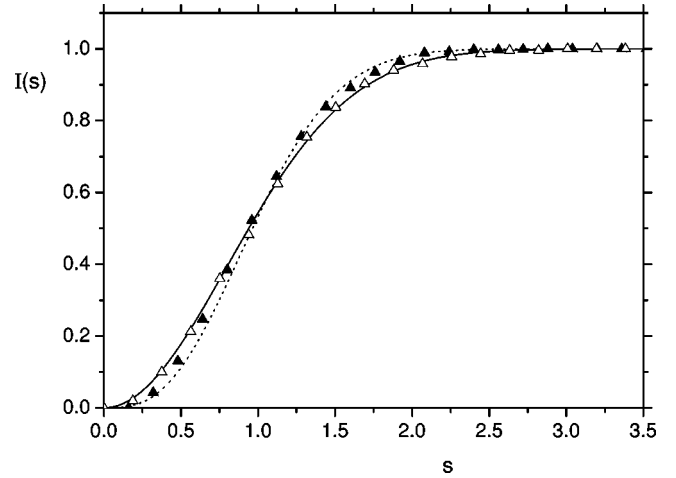


FIG. 6. Integrated nearest neighbor spacing distribution averaged for eight realizations of the microwave graphs with Faraday isolators (solid triangles) is compared with the averaged results for the microwave graphs without the isolators (open triangles) and theoretical prediction for GOE (solid line) and GUE (dashed line). In both cases experimental results were obtained for the frequency range 3.5–7.5 GHz.

directed bond—can be described by means of a filter factor which damps the wave moving in one direction. In the numerical analysis of the directed graphs we have assumed that by measuring the reflection spectra of the graphs we are rather probing the graphs as closed systems by some coupling, which is weak enough, not to influence the internal dynamics of the systems.

We introduce the connectivity matrix D of a directed graph, which does not need to be symmetric. With any directed graph Γ one may associate a bidirectional graph G with the same number of vertices. Its connectivity matrix C is symmetric,

$$C_{ij} = \max(D_{ij}, D_{ji}). \quad (11)$$

The number B of bonds in the graph G is equal to $B = \frac{1}{2} \sum_{ij} C_{ij}$. To be able to filter some waves propagating in one direction while preserving those moving in the opposite direction we will use a bond scattering technique of analyzing spectra of graphs, similar to this introduced by Kottos and Smilansky [12]. Consider a plain wave $\Psi_{j'n}(x) = e^{-ikx}$ coming from the vertex j' to the vertex n . It is scattered into all bonds going out from the vertex n , for which $C_{nj} \neq 0$,

$$\Phi_{nj}(x) = \delta_{jj'} e^{-ikx} + \sigma_{jj'}^{(n)} e^{ikx}. \quad (12)$$

The vertex scattering matrix $\sigma_{jj'}^{(n)}$ is completely determined, if we assume Neumann boundary conditions (9), which imply

$$\sigma_{jj'}^{(n)} = C_{j'n} C_{nj} (-\delta_{jj'} + 2/v_n). \quad (13)$$

Here v_n denotes the number of bonds meeting at the n th vertex, also called the *valency* of the vertex. Elements of $\sigma_{jj'}^{(n)}$ for all vertex n combine to the entire bond transition matrix of the graph G

$$T_{jl,mm} = \delta_{ln} C_{jl} C_{nm} \sigma_{jm}^{(l)}, \quad (14)$$

which describe the changes of amplitudes of waves propagating in each bond of the graph (in both directions) after one event of scattering on vertices. The matrix dimension is equal to twice the number of bonds B in the graph. To take into account the presence of the Faraday isolators we make use of the connectivity matrix D of the directed graph Γ , and introduce a diagonal $2B \times 2B$ matrix $\Lambda(k)$

$$\Lambda_{jl,j'l'}(k) = \delta_{jj'} \delta_{ll'} D_{jl} e^{ikL_{jl}}, \quad (15)$$

where the phase factor describes the free propagation along the bond (jl) of length L_{jl} . By definition, the element D_{jl} is equal to zero for bonds which do not belong to the directed graph Γ . The effect of absorption of the microwave field by microwave cables can be easily taken into account by modifying the matrix $\Lambda_{jl,j'l'}(k)$ given by Eq. (15) to the form $\delta_{jj'} \delta_{ll'} D_{jl} e^{(ik - \beta \sqrt{k})L_{jl}}$, where β is the absorption coefficient. The total evolution of the vector of wave amplitudes of length $2B$ is given by the bond scattering matrix

$$S(k) = \Lambda(k)T. \quad (16)$$

The matrix $S(k)$ is subunitary, since it is obtained by putting to zero some elements of a unitary matrix. We denote the eigenvalues of $S(k)$ by $\lambda_j(k)$, all of $\lambda_j(k)$ are located in (or at) the unit circle, $|\lambda_j(k)| \leq 1$. The equation for the eigenmodes of the quantum graph

$$\det(S(k) - 1) = 0 \quad (17)$$

may have no real solution. In our experimental setup the graph is driven by the microwave generator. We are interested, for which wave vectors k the resonant driving of the graph will appear. We analyze the stationary state of the system, in which an arbitrary number p of scattering processes take place and decompose it in the eigenbasis of $S(k)$. The amplitudes of each mode become an infinite superposition of waves scattered p times, so the enhancement factor $r_j(k)$ of the j th mode reads

$$r_j(k) = \sum_{p=0}^{\infty} [\lambda_j(k)]^p = \frac{1}{1 - \lambda_j(k)}, \quad (18)$$

where $\lambda_j(k)$ are the eigenvalues of the bond scattering matrix $S(k)$. Since each eigenmode may contribute to the resonant dissipation in the system, we approximate the total response function of the graph by the average enhancement factor [the mean of $r_j(k)$]

$$r(k) = \frac{1}{2B} \sum_{j=1}^{2B} r_j(k) = \frac{1}{2B} \sum_{j=1}^{2B} \frac{1}{1 - \lambda_j(k)}. \quad (19)$$

Maxima of this function, which occur if one of the eigenvalues $\lambda_j(k)$ is close to unity, identify resonant values of the wave vector k . We analyzed the function $r(k)$ generated for parameters of the system as used in the experiment and studied numerically the statistics of its maxima.

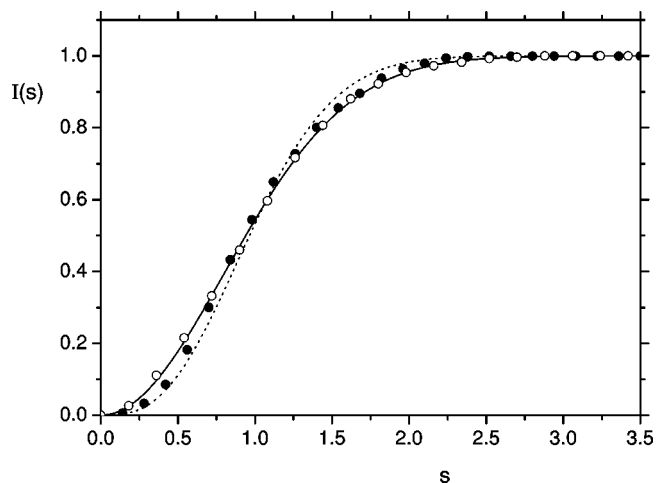


FIG. 7. Numerically calculated integrated nearest neighbor spacing (INNS) distributions averaged for 20 realizations of the directed graphs (solid circles) is compared with the averaged results for the bidirectional graphs (open circles). Calculations were performed in the frequency range 0–20 GHz. Numerical results for the INNS distributions are compared with theoretical predictions for GOE (solid line) and GUE (dashed line).

Using this approach we calculated approximated eigenfrequencies of 20 directed graphs in the frequency range 0–20 GHz. As in the experimental realization, only one bond was assumed to be directed. Numerical search for the eigenfrequencies was performed for two sets of directed graphs with five different lengths of a directed bond b (see Fig. 1 for the assignment of the letters to the bonds of the graph). The other bonds of the graphs were bidirectional and within the set were kept fixed. The same number of numerical calculations were also done for two sets of directed graphs with the varied length of the directed bond d . Figure 7 shows the integrated nearest neighbor spacing distribution averaged for 20 realizations of the directed graphs in the frequency range 0–20 GHz. Together 3207 eigenfrequencies were used in the calculations of the INNS distribution. In this case we decided not to put the experimental and theoretical data on one plot, to emphasize that the results are based on different statistics and cannot be directly compared. However, it is justified to compare these numerical results obtained for the directed graphs (solid circles) with the numerical data obtained in the frequency range 0–20 GHz for 20 realizations of standard (bidirectional) graphs (empty circles). In this case 4641 eigenfrequencies were used in the calculations of the INNS distribution. Theoretical predictions for GOE and GUE, denoted by solid and dashed curve, respectively, suggest that the INNS spectral statistics for directed graphs deviate at small spacings from the GOE curve and become closer to the GUE predictions. This result confirms also our experimental findings for the microwave directed graphs.

In summary, we show that quantum graphs with Neumann boundary conditions can be simulated experimentally by microwave networks. Bidirectional microwave graphs, i.e., cir-

cuits without Faraday isolators, simulate quantum graphs with time reversal symmetry. The results for the directional microwave graphs with Faraday isolators, for which the time reversal symmetry is broken, indicate that their certain characteristics such as the integrated nearest neighbor spacing distribution can significantly differ from the RMT prediction

for GOE, approaching the results characteristic of GUE.

This work was partially supported by KBN Grant Nos. 2 P03B 047 24 and 1 P03B 042 26. We would like to thank Professor Marek Kuś and Professor Petr Šeba for valuable discussions.

-
- [1] L. Pauling, *J. Chem. Phys.* **4**, 673 (1936).
 [2] H. Kuhn, *Helv. Chim. Acta* **31**, 1441 (1948).
 [3] C. Flesia, R. Johnston, and H. Kunz, *Europhys. Lett.* **3**, 497 (1987).
 [4] R. Mitra and S. W. Lee, *Analytical Techniques in the Theory of Guided Waves* (Macmillan, New York, 1971).
 [5] E. L. Ivchenko and A. A. Kiselev, *JETP Lett.* **67**, 43 (1998).
 [6] J. A. Sanchez-Gil, V. Freilikher, I. Yurkevich, and A. A. Maradudin, *Phys. Rev. Lett.* **80**, 948 (1998).
 [7] Y. Imry, *Introduction to Mesoscopic Systems* (Oxford University Press, New York, 1996).
 [8] D. Kowal, U. Sivan, O. Entin-Wohlman, and Y. Imry, *Phys. Rev. B* **42**, 9009 (1990).
 [9] Y. Avishai and J. M. Luck, *Phys. Rev. B* **45**, 1074 (1992).
 [10] T. Nakayama, K. Yakubo, and R. L. Orbach, *Rev. Mod. Phys.* **66**, 381 (1994).
 [11] T. Kottos and U. Smilansky, *Phys. Rev. Lett.* **79**, 4794 (1997).
 [12] T. Kottos and U. Smilansky, *Ann. Phys. (N.Y.)* **274**, 76 (1999).
 [13] T. Kottos and U. Smilansky, *Phys. Rev. Lett.* **85**, 968 (2000).
 [14] T. Kottos and H. Schanz, *Physica E (Amsterdam)* **9**, 523 (2003).
 [15] T. Kottos and U. Smilansky, *J. Phys. A* **36**, 3501 (2003).
 [16] F. Barra and P. Gaspard, *J. Stat. Phys.* **101**, 283 (2000).
 [17] G. Tanner, *J. Phys. A* **33**, 3567 (2000).
 [18] G. Tanner, *J. Phys. A* **34**, 8485 (2001).
 [19] P. Pakoński, K. Życzkowski, and M. Kuś, *J. Phys. A* **34**, 9303 (2001).
 [20] P. Pakoński, G. Tanner, and K. Życzkowski, *J. Stat. Phys.* **111**, 1331 (2003).
 [21] R. Blümel, Yu Dabaghian, and R. V. Jensen, *Phys. Rev. Lett.* **88**, 044101 (2002).
 [22] H. J. Stöckmann and J. Stein, *Phys. Rev. Lett.* **64**, 2215 (1990).
 [23] S. Sridhar, *Phys. Rev. Lett.* **67**, 785 (1991).
 [24] H. Alt, H.-D. Gräf, H. L. Harner, R. Hofferbert, H. Lengeler, A. Richter, P. Schardt, and A. Weidenmüller, *Phys. Rev. Lett.* **74**, 62 (1995).
 [25] P. So, S. M. Anlage, E. Ott, and R. N. Oerter, *Phys. Rev. Lett.* **74**, 2662 (1995).
 [26] U. Stöffregen, J. Stein, H.-J. Stöckmann, M. Kuś, and F. Haake, *Phys. Rev. Lett.* **74**, 2666 (1995).
 [27] F. Haake, M. Kuś, P. Šeba, H.-J. Stöckmann, and U. Stöffregen, *J. Phys. A* **29**, 5745 (1996).
 [28] L. Sirko, P. M. Koch, and R. Blümel, *Phys. Rev. Lett.* **78**, 2940 (1997).
 [29] E. Doron, U. Smilansky, and A. Frenkel, *Phys. Rev. Lett.* **65**, 3072 (1990).
 [30] E. Persson, I. Rotter, H.-J. Stöckmann, and M. Barth, *Phys. Rev. Lett.* **85**, 2478 (2000).
 [31] S. Deus, P. M. Koch, and L. Sirko, *Phys. Rev. E* **52**, 1146 (1995).
 [32] C. Dembowski, B. Dietz, H.-D. Gräf, A. Heine, T. Papenbrock, A. Richter, and C. Richter, *Phys. Rev. Lett.* **89**, 064101 (2002).
 [33] D. S. Jones, *Theory of Electromagnetism* (Pergamon Press, Oxford, 1964), p. 254.
 [34] L. D. Landau and E. M. Lifshitz, *Electrodynamics of Continuous Media* (Pergamon Press, Oxford, 1960).
 [35] G. Goubau, *Electromagnetic Waveguides and Cavities* (Pergamon Press, Oxford, 1961).
 [36] R. Blümel and U. Smilansky, *Phys. Rev. Lett.* **60**, 477 (1988).
 [37] P. Kuchment and H. Zeng, *J. Math. Anal. Appl.* **258**, 671 (2001).
 [38] J. Rubinstein and M. Schatzman, *Arch. Ration. Mech. Anal.* **160**, 271 (2001).
 [39] F. Haake, *Quantum Signatures of Chaos*, 2nd ed. (Springer, Berlin, 2000).
 [40] H.-J. Stöckmann, *Quantum Chaos — An Introduction* (Cambridge University Press, Cambridge, 1999).
 [41] Sz. Bauch, A. Błędowski, L. Sirko, P. M. Koch, and R. Blümel, *Phys. Rev. E* **57**, 304 (1998).
 [42] M. V. Berry, *Proc. R. Soc. London, Ser. A* **400**, 229 (1985).